Research in Astronomy and Astrophysics, 24:125012 (9pp), 2024 December https://doi.org/10.1088/1674-4527/ad9198

JWST Observations Constrain the Time Evolution of Fine Structure Constants and Dark Energy-electromagnetic Coupling

Ze-Fan Wang[1,2], Lei Lei[1,2], Lei Feng[1,2], and Yi-Zhong Fan[1,2]
[1] Key Laboratory of Dark Matter and Space Astronomy, Purple Mountain Observatory, Chinese Academy of Sciences, Nanjing 210033, China; leilei@pmo.ac.cn, fenglei@pmo.ac.cn
[2] School of Astronomy and Space Science, University of Science and Technology of China, Hefei 230026, China
Received 2024 July 01; revised 2024 October 29; accepted 2024 November 08; published 2024 December 5

Abstract

It was hypothesized in the literature that some physical parameters may be time-evolving and the astrophysical data can serve as a probe. Recently, the James Webb Space Telescope (JWST) released its early observations. In this work, we select the JWST spectroscopic observations of the high redshift ($z > 7.1$) galaxies with strong [O III] ($\lambda = 4959$ Å and 5007 Å in the rest frame) emission lines to constraint the evolution of the fine structure constant (α). With the spectra from two galaxies at redshifts of 7.19 and 8.47, the deviation of α from its fiducial value is found to be as small as $0.44^{+8.4+1.7}_{-8.3-1.7} \times 10^{-4}$ and $-10.0^{+18+1.5}_{-18-1.5} \times 10^{-4}$, respectively (the first error is statistical and the latter is systematic). The combination of our results with the previous data reveals that $\frac{1}{\alpha}\frac{d\alpha}{dt} = 0.30^{+4.5}_{-4.5} \times 10^{-17}\,\mathrm{yr}^{-1}$. Clearly, there is no evidence for a cosmic evolution of α. The prospect of further constraining the time evolution of α is also discussed. The scalar field of dark energy is hypothesized to drive the acceleration of the universe's expansion through an interaction with the electromagnetic field. By integrating the observational data of the fine-structure constant variation, $\frac{\Delta\alpha}{\alpha}(z)$, we have established a stringent upper limit on the coupling strength between dark energy and electromagnetism. Our analysis yields $\zeta \leqslant 3.92 \times 10^{-7}$ at the 95% confidence level, representing the most stringent bound to date.

Key words: cosmology: observations – (cosmology:) dark energy – galaxies: high-redshift

1. Introduction

Fundamental physical constants are one facet of nature's laws, but are they really non-evolving in the universe? Dirac (1937) proposed the famous large-number coincidence, suggesting an association between fundamental constants and the current status of the universe. About one decade after that, Teller (1948) argued that the time variation of gravitational constant (G) seems impossible due to the ecosystems on our Earth. Nevertheless, further probe is still necessary to check whether there is the cosmic evolution of the physical constants or not. One good target is the fine-structure constant which can be expressed as $\alpha = \frac{e^2}{4\pi\varepsilon_0\hbar c}$, where e is the electron charge, ε_0 is the vacuum permittivity, $\hbar$ is the reduced Planck constant, and c is the speed of light in a vacuum. The numerical value of this dimensionless constant is found to be $\alpha^{-1} = 137.035999206(11)$ (Morel et al. 2020). A reliable identification of a deviation of α from such a standard value would suggest the presence of new physics.

In the middle of the 20th century, Stanyukovich (1963) and Gamow (1967) introduced the idea of time variation of α in cosmology. Dyson (1967) deduced that the time variation of e is less than $1/1600$ during the history of Earth from the terrestrial existence of the nuclei Re^{187} and Os^{187}, but Gamow (1967) did give suggestions on the detection of a time-varying α through astronomical sources. Savedoff (1956) first analyzed the spectral fine-structure of the emission lines of [N II] and [Ne III] in the spectrum of a nearby Seyfert galaxy. Astronomers have since been clear that the upper bound of the relative variation $\Delta\alpha/\alpha$ and the time variation $\frac{1}{\alpha}\frac{d\alpha}{dt}$ in our local universe must be extremely small (Lee et al. 2005; Petrov et al. 2006; Rosenband et al. 2008; Wilczynska et al. 2015; Martins & Pinho 2017). Consequently, modern observations focus on high redshift celestial bodies to explore the potential change of α in the early universe (Alves et al. 2018; Wilczynska et al. 2020). Thanks to the successful launch and outstanding performance of the James Webb Space Telescope (JWST), astronomers are now able to catch a glimpse of the young generation of galaxies and stars at very high redshifts. Recently, Jiang et al. (2024b, 2024a)[3] constrained the high redshift evolution of the fine-structure constant with galaxy spectra, improving high redshift research on the electromagnetic force. With the JWST data, the possible cosmic evolution of α and dark energy-electromagnetic (DE-EM) coupling can be further explored, which is the main purpose of this work.

[3] After the initial submission of our manuscript for publication on 2024 May 4, Jiang et al. (2024a) appeared in arXiv. In our analysis, just the high-resolution spectral data have been taken into account, while Jiang et al. (2024a) also analyzed the medium resolution data.

In this paper we probe the cosmic variation of α using the [O III] $\lambda\lambda$ 4959,5007 doublet emission lines (hereafter [O III]) of the very high redshift ($z > 7$) galaxies. These two lines do not suffer from serious absorption and are strong enough to be reliably measured in the infrared spectrum of the high redshift objects. We concentrate on two sources at the redshifts of $z = 8.47$ and 7.19 from the JWST Advanced Deep Extragalactic Survey (JADES; Bunker et al. 2023; Eisenstein et al. 2023). The structure of this work is as follows. In Section 2, we introduce our sample, discuss the advantages of the [O III] doublet to probe the possible variations of α, and outline our method for fitting the spectroscopic data. Section 3 covers the calculation of the variation of α and the presentation of our key findings. We will wrap up and delve into the implications of our results in Section 4. In Section 4, we constrain the time evolution of the fine-structure constant and DE-EM coupling. Additionally, we address potential contamination issues associated with the [O III] method utilized in this study. Throughout this work, we adopt a Λ-CDM model with $H_0 = 67.4\,\mathrm{km\,s^{-1}\,Mpc^{-1}}$, $\Omega_m = 0.3$, and $\Omega_\Lambda = 0.7$ (Planck Collaboration et al. 2020).

2. Sample Selection and Method

In this section, we will first introduce our sample selection in JADES, and then we will briefly review different methods of testing the potential of varying α and introduce the [O III] method as a probe of variation of α. Lastly, we will describe our Markov Chain Monte Carlo (MCMC) technique to fit the galaxy [O III] spectra.

2.1. Sample Selection

In this work, we only use the JWST spectroscopic observations with F290LP-G395H filter because of its high-resolution ($R = 1900\sim3600$) and lower systematic uncertainty. We scan through the public JADES catalog of NIRSpec Clear-Prism Line Fluxes and NIRSpec Gratings Line Fluxes to find the sources with redshift (z) over 7.1, and set a signal-to-noise ratio (SNR) test. Letting the SNR for the [O III]λ5007 line intensity be at least 8:1, which means the area under the 5007 Å line is measured to an accuracy of $\pm$12.5%, we finally select the two emission-line galaxies (ELGs) and their NIRSpec ID are 00008013 and 10013905, respectively.

2.2. Probe the α Variation with the [O III] Doublet

In the early exploration of the time variation of α, astronomers initially adopted the emission lines of nearby quasars (Savedoff 1956; Bahcall & Salpeter 1965) to establish an upper limit. However, this approach was soon abandoned because the broad emission lines can be influenced by the central supermassive black holes and researchers decided to focus on studying quasar absorption lines to understand the time dependence of α (Bahcall et al. 1967). Subsequently, the alkali-doublet (AD) method was developed to analyze absorption lines from gas clouds utilizing luminous quasars as reference points. While effective, the AD method does not fully exploit the potential information in quasar spectra, leading to the development of the many-multiplet (MM) method. This method leverages multiple atomic transitions from various multiplets and ionization stages to enhance sensitivity in probing α's time dependence (Webb et al. 1999, 2001). However, the MM method introduces uncertainties due to the complex many-body atomic theory involved (Bahcall et al. 2004).

Thus, we take the [O III] emission lines in ELGs as a probe of varying α in the early universe. There are some advantages of using [O III] to probe the varying α. First, the doublet lines have a significantly wider wavelength separation of around 50 Å, which is approximately ten times larger than the separation seen in most fine-structure doublet lines. Besides, the [O III] doublet lines are much narrower and cleaner in ELGs, and sometimes the strongest in spectra, so it is easy for us to get high SNR data of the [O III]. The whole procedure of detection is also simple and straightforward without making assumptions in MM method (Bahcall et al. 2004). High redshift observations ($z \gtrsim 7$) pose challenges for traditional methods like MM and AD due to neutral hydrogen absorption and limited heavy elements in the early universe (Miralda-Escudé 1998; Robertson et al. 2010; Wise 2019). While ELGs offer a promising avenue for studying α variation, the scarcity of high-resolution ELG spectra hampers their widespread use.

Considering non-relativistic approximation, the observed separation of wavelength ($\Delta\lambda = \lambda_1 - \lambda_2$) of the doublet is proportional to the fine-structure constant: $\Delta\lambda/\bar{\lambda} \propto \alpha^2$. Here $\bar{\lambda}$ is the average of the wavelengths. Then the anomaly of the fine-structure constant $\Delta\alpha/\alpha$ is calculated by

$$\frac{\Delta\alpha}{\alpha} = \sqrt{\frac{\Delta\lambda(z)/\bar{\lambda}(z)}{\Delta\lambda(0)/\bar{\lambda}(0)}} - 1, \tag{1}$$

where z stands for the source redshift. The denominator, the present-day value of $\Delta\lambda/\bar{\lambda}$, is (Peck & Reeder 1972; Moorwood et al. 1980; Pettersson 1982; Bahcall et al. 2004)

$$R(0) = \frac{\Delta\lambda(0)}{\bar{\lambda}(0)} = 4.80967 \times 10^{-3}[1 \pm 0.000\,01]. \tag{2}$$

2.3. MCMC Method to Fit the Spectrum

In order to fit the spectroscopic data, we construct a model to describe the shape of [O III] lines and the continuum component in the spectra, which reads

$$F(x|a, b, \lambda_2, \Delta\lambda, n_1, n_2, s_1, s_2) = -10^a x + 10^b + \frac{10^{n_1 - s_1}}{\sqrt{2\pi}} e^{\frac{-(x-(\lambda_2-\Delta\lambda))^2}{(2\times10^{s_1})^2}} + \frac{10^{n_2-s_2}}{\sqrt{2\pi}} e^{\frac{-(x-\lambda_2)^2}{(2\times10^{s_2})^2}}, \tag{3}$$

where a is the log-slope of the continuum, b is the log-intercept of the continuum, λ_2 is the wavelength of the [O III]λ5007 line,

Table 1
The A Priori Ranges of the Eight Free Parameters

Parameter	Type	Range
a	Uniform	$(-23.0, 0)$
b	Uniform	$(-29, 0)$
$\frac{\lambda_{5007}}{(1+z)}$	Uniform	(4996.84, 5016.84)
$\frac{\Delta\lambda}{(1+z)}$	Uniform	(38, 58)
n_1	Uniform	$(-24.5, -21)$
n_2	Uniform	$(-23, -20)$
s_1	Uniform	$(-4, -1.5)$
s_2	Uniform	$(-4, -1.5)$

Table 2
Final Parameter Estimation of the Two [O III] ELGs with 1σ of the Posterior as Statistical Uncertainty

Parameter	NIRSpec 10013905	NIRSpec 00008013
λ_2 (μm)	$4.11^{+0.0000267}_{-0.0000266}$	$4.74^{+0.0000668}_{-0.0000663}$
$\Delta\lambda$ (μm)	$0.0393^{+0.0000662}_{-0.0000649}$	$0.0453^{+0.000162}_{-0.000164}$

$\Delta\lambda$ is the wavelength separation between the two [O III]λ4959 and [O III]λ5007 fine-structure lines, n_1 and s_1 are the two parameters amplitude and 1σ width of the [O III]λ4959 Gaussian emission line profile respectively, and n_2 and s_2 are the same components of the [O III]λ5007 emission line profile. The slope of the spectral continuum emission is negative, which is because of the strong ultraviolet (UV) radiation continuum emission. This UV radiation is a result of their vigorous star formation activities (Topping et al. 2024). One linear function is to fit the background and two Gaussian-like functions are designed for fitting the [O III] line shape. There are eight free parameters in this model and we define an objective function

$$\chi^2 = \sum_{i=1}^{N} \frac{(y_i - F_i)^2}{\sigma_y^2}, \tag{4}$$

and a log-likelihood used to estimate the posterior probabilities

$$-2 \ln \mathcal{L} = \chi^2. \tag{5}$$

Our goal is to maximize this $\mathcal{L}$ and we deploy the MCMC technique to estimate all the eight parameters with the help of the `emcee` package (Foreman-Mackey et al. 2013). The a priori ranges of the eight free parameters are listed in Table 1.

After 50,000 runs, we put the posterior parameters into the a priori and run another 50,000 times. Cornerplots of the full set of posterior distributions are shown below in the Appendix and the final parameter estimations (Table 2) are also tabulated.

3. Results

In this section, we will present the final results of the best-fit spectral profiles, and calculate $\Delta\alpha/\alpha$. Substituting the fitting results in Table 2 to Equation (1), we work out the result of $\frac{\Delta\alpha}{\alpha}$, and the best-fit line profiles are displayed in Figures 1 and 2 for our two sources.

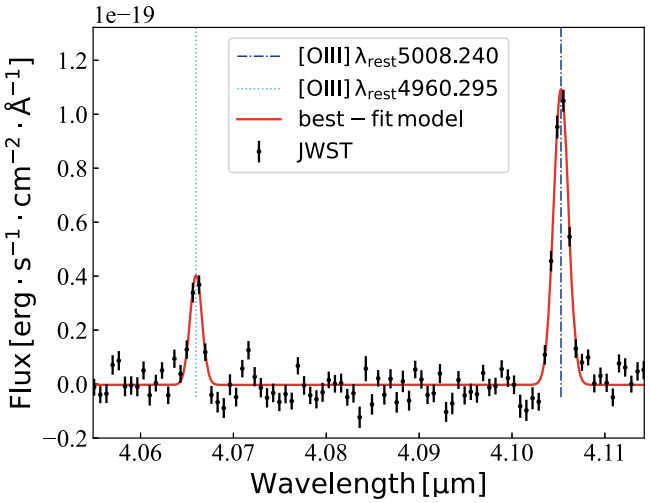

Figure 1. The best-fit model and JWST-NIRSpec data of NIRSpec 10013905 [O III] emission lines. The black points with error bars are the observed JWST spectrum data. The red line is the best-fit model of the [O III] doublet emission lines. The dotted line in cyan and dash-dotted line in blue are best-fit lines' wavelengths of [O III]λ4959 and [O III]λ5007 lines respectively.

However, we also need to take into account the systematic uncertainties. The systematic uncertainty due to the spectral resolution is $\delta\lambda = \frac{0.00066498\ (\mu\mathrm{m})}{50} = 1.33 \times 10^{-5}\ (\mu\mathrm{m})$ in this wavelength range, where the factor $\frac{1}{50}$ is the JWST spectral calibration error (Jakobsen et al. 2022). Here, the systematic error is attributed to the imaging calibration of the NIRSpec filter and grating wheels.[4] Because the systematic errors of $\Delta\lambda$ and λ_2 are from the same resolution limit, these two parameters have the same systematic uncertainty equal to $\delta\lambda$. Throwing these factors into the propagation equation of uncertainty

$$\begin{aligned}\sigma^2_{\frac{\Delta\alpha}{\alpha}} = &\frac{\Delta\lambda}{4R^3(0)(-\Delta\lambda + 2\lambda_2)}\sigma^2_{R(0)} \\ &+ \frac{\Delta\lambda}{R(0)(-\Delta\lambda + 2\lambda_2)^3}\sigma^2_{\lambda_2} \\ &- \frac{\lambda_2^2}{\Delta\lambda(\Delta\lambda - 2\lambda_2)^3 R(0)}\sigma^2_{\Delta\lambda},\end{aligned} \tag{6}$$

we have $0.44^{+8.4(\mathrm{stat})+1.7(\mathrm{sys})}_{-8.3(\mathrm{stat})-1.7(\mathrm{sys})} \times 10^{-4}$ and $-10.0^{+18(\mathrm{stat})+1.5(\mathrm{sys})}_{-18(\mathrm{stat})-1.5(\mathrm{sys})} \times 10^{-4}$ for these two sources NIRSpec 10013905 and NIRSpec 00008013, respectively. The larger uncertainty is the systematic one. The smaller one is 1σ statistical error from the fitting. It is apparent that the systematic uncertainty plays the dominant

[4] The relative wavelength calibration, which takes into account the effects of dispersion, is a complex process and has not yet yielded robust results. Consequently, we have estimated the systematic uncertainty associated with the imaging calibration of the NIRSpec filter and grating wheels.

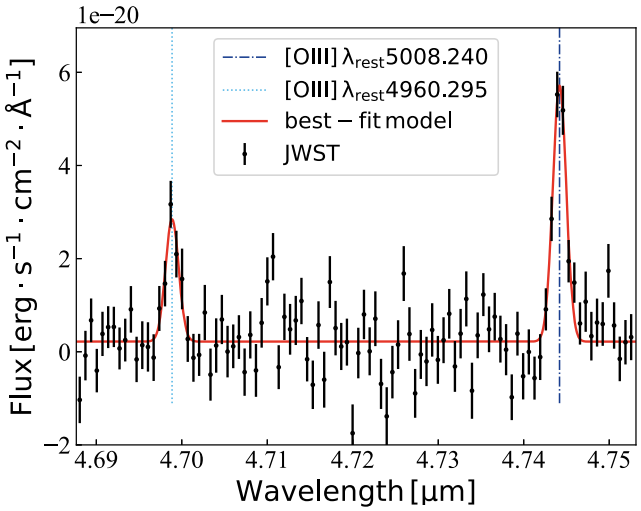

Figure 2. Same as Figure 1, but for the source NIRSpec 00008013.

role in constraining the α variation. Thus, higher resolution observations are needed for further investigation. Or, we have to identify more distinct emission lines in the spectra of the objects in the early universe.

4. Conclusions and Discussions

To conclude, we utilized the farthest observations of the [O III] emission lines to constrain the variability of $\frac{\Delta\alpha}{\alpha}$. This choice was primarily due to the strength of these two lines, making them detectable in the high redshift universe, and the separation between the lines wide enough for the instrument to capture. These emission lines act as a natural probe for researchers to explore the possibility of a changing α. Our findings suggest that α has remained nearly constant since the early universe.

4.1. Constraint on the Time Evolution of the Fine-Structure Constant

Combining the results before, the final sample of $\frac{\Delta\alpha}{\alpha}$ spans the redshift range of $0.2 < z < 8.5$. The data are illustrated in Figure 4. The cited data at lower redshifts $0.2 < z < 7.1$ are from the works (King et al. 2012; Wilczynska et al. 2015; Martins & Pinho 2017; Wilczynska et al. 2020).

We use these data to estimate the relative time variance of the fine-structure constant ($\frac{1}{\alpha}\frac{d\alpha}{dt}$) via the procedure developed by Bahcall et al. (2004). We fit the linear function of time

$$\frac{\Delta\lambda(t(z))/\bar{\lambda}(t(z))}{\Delta\lambda(0)/\bar{\lambda}(0)} = 1 + \mathrm{SH}_0 t. \tag{7}$$

Here we use the well-known expression

$$t = \int_0^z \frac{(1+z')^{-1}dz'}{\sqrt{(1+z')(1+\Omega_m z') - z'(2+z')\Omega_\Lambda}}, \tag{8}$$

to convert z to t (Mukhanov 2005). The slope S in Equation (7) is

$$S = \frac{1}{H_0\alpha^2}\left(\frac{d\alpha^2}{dt}\right) = \frac{2}{H_0\alpha}\frac{d\alpha}{dt}. \tag{9}$$

We determine the parameters with the MCMC method once again. Our result is

$$\frac{1}{\alpha}\frac{d\alpha}{dt} = 0.30^{+4.5}_{-4.5} \times 10^{-17}\,\mathrm{yr}^{-1}.$$

The statistical uncertainty is 1σ (the bold ones are 2σ) and the posterior distribution is shown underneath in Appendix. It again indicates a time-independent α in our universe.

4.2. Constraint on Dark Energy Coupling with Electromagnetism

The coupling between dark energy and electromagnetism could potentially lead to observable phenomena, such as the temporal evolution of the fine-structure constant (Avelino et al. 2006; Thompson 2013; Calabrese et al. 2014; Chen et al. 2019). The interaction between the dark energy scalar field (ϕ) and electromagnetism (F) can be described by a gauge kinetic function $B_{F(\phi)}$ (Calabrese et al. 2014)

$$\mathcal{L}_{\phi F} = -\frac{1}{4}B_F(\phi)F_{\mu\nu}F^{\mu\nu}. \tag{10}$$

This gauge kinetic function is linearly dependent on the scalar field (Nunes & Lidsey 2004; Avelino et al. 2006; Vielzeuf & Martins 2014)

$$B_F(\phi) = 1 - \zeta\sqrt{8\pi G}\,(\phi - \phi_0), \tag{11}$$

where ζ represents the coupling strength between the scalar dark energy field and the electromagnetic field.

Consequently, the variation of the fine-structure constant α due to the DE-EM coupling is expressed as (Calabrese et al. 2014)

$$\frac{\Delta\alpha}{\alpha} \equiv \frac{\alpha - \alpha_0}{\alpha_0} = \zeta\sqrt{8\pi G}\,(\phi - \phi_0). \tag{12}$$

The temporal evolution of the fine-structure constant α, attributed to the coupling between dark energy and electromagnetism, can be reformulated as follows (Calabrese et al. 2014)

$$\frac{\Delta\alpha}{\alpha}(z) = \zeta\int_0^z \sqrt{3\Omega_\phi(z)[1+w(z)]}\,\frac{dz'}{1+z'}. \tag{13}$$

There is no simple analytical solution to the equation of state of the dark energy scalar field mentioned above, and most of the previous work (e.g., Nunes & Lidsey 2004; Avelino et al. 2006) has used higher-order polynomials for fitting or modeling, and some works (e.g., Calabrese et al. 2014; Vielzeuf & Martins 2014) assumed a parameterized Chevallier–Polarski–Linder (CPL) dark energy equation of state, and then performed a

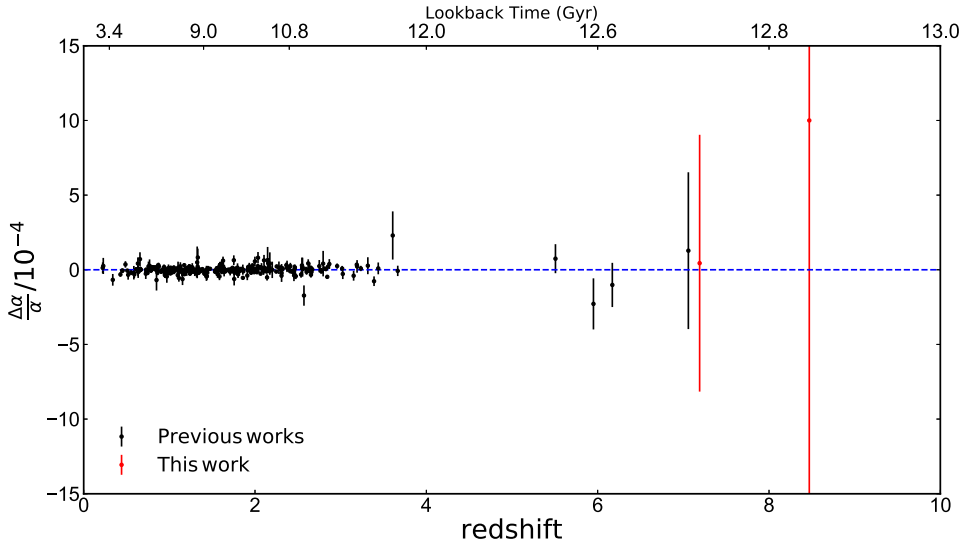

Figure 3. Direct measurements of $\frac{\Delta\alpha}{\alpha}$ in different cosmic epochs. The red data points are from best-fit [O III] results of the two JWST ELGs NIRSpec 10013905 and NIRSpec 00008013 in this work. The others in black are from different references with MM methods (King et al. 2012; Wilczynska et al. 2015; Martins & Pinho 2017; Wilczynska et al. 2020).

parameterized fitting of the change of the fine structure constant. To constrain the coupling strength ζ between dark energy and electromagnetism, we adopt the CPL parameterization of the dark energy equation of state, which features two adjustable parameters, w_0 and w_a (Chevallier & Polarski 2001; Linder 2003)

$$w(z) = w_0 + w_a \frac{z}{1+z}. \tag{14}$$

The fractional density of dark energy in the universe is articulated by

$$\Omega_\phi(z) = \Omega_{\phi 0}(1+z)^{3(1+w_0+w_a)} e^{-3w_a \frac{z}{1+z}}. \tag{15}$$

The black data points in Figure 3 represent previous findings, while the current constraints from the JWST on $\frac{\Delta\alpha}{\alpha}(z)$ are depicted as red error bars.

We have integrated the latest JWST [O III] measurement of $\Delta\alpha/\alpha$ with prior measurements cited in King et al. (2012), Wilczynska et al. (2015), Martins & Pinho (2017), Wilczynska et al. (2020) to establish constraints on the DE-EM coupling as defined by Equations (11)–(15). During the fitting process, we assigned Gaussian priors to the parameters w_0 and w_a: $\mathcal{G}(-0.957 \pm 0.08)$ for w_0 and $\mathcal{G}(-0.29 \pm 0.3)$ for w_a, reflecting observational constraints from Planck18+SNe+BAO (Planck Collaboration et al. 2020). For the DE-EM coupling strength ζ, we imposed a log-flat prior with an upper limit of $\log_{10}\zeta = 1.0$ and a lower limit of $\log_{10}\zeta \approx -38.2$. This lower boundary corresponds to the dimensionless gravitational fine-structure constant $\alpha_g = \frac{G_N m_p^2}{\hbar c} \approx 6 \times 10^{-39}$ as derived in Moss et al. (2010).

The colored lines in Figure 4 illustrate the evolution of the fine-structure constant according to the DE-EM coupling model. The lines with various line styles represent the variation of $\frac{\Delta\alpha}{\alpha}(z)$ for different strengths of DE-EM coupling. The current collective data of $\frac{\Delta\alpha}{\alpha}(z)$ has led to a stringent constraint on the DE-EM coupling strength ζ

$$\zeta \leqslant 3.92 \times 10^{-7} \text{ (at } 95\% \text{ Confidence Level)}.$$

This constraint is contingent upon the utilization of the CPL dark energy equation of state. Additionally, we have examined the constraints for the dark-energy-electromagnetic coupling model under various types of priors, such as flat priors. The outcomes indicate that the results are consistent with those aforementioned, with the constraints derived from different priors exhibiting similar magnitudes (i.e., orange solid line versus blue dotted line in Figure 4). The current 95% limit is about three orders of magnitude stronger than the results of other previous work (e.g., $\zeta < 10^{-3}$ obtained by Olive & Pospelov 2002 with cosmic microwave background (CMB)).

4.3. Excluding the Potential Contamination of the [O III] Method

4.3.1.

Although the [O III] emission lines have advantages in testing the variation of α in the high redshift universe (i.e., see Section 2.2), they may be not precise because of the pollution from galaxies with active galactic nuclei (AGNs or quasars). The quasar emission lines tend to be broad, which is not ideal for precise measurement of radial velocity. While the [O III] lines in quasars are not as broad as lines like [C IV] and [Mg II],

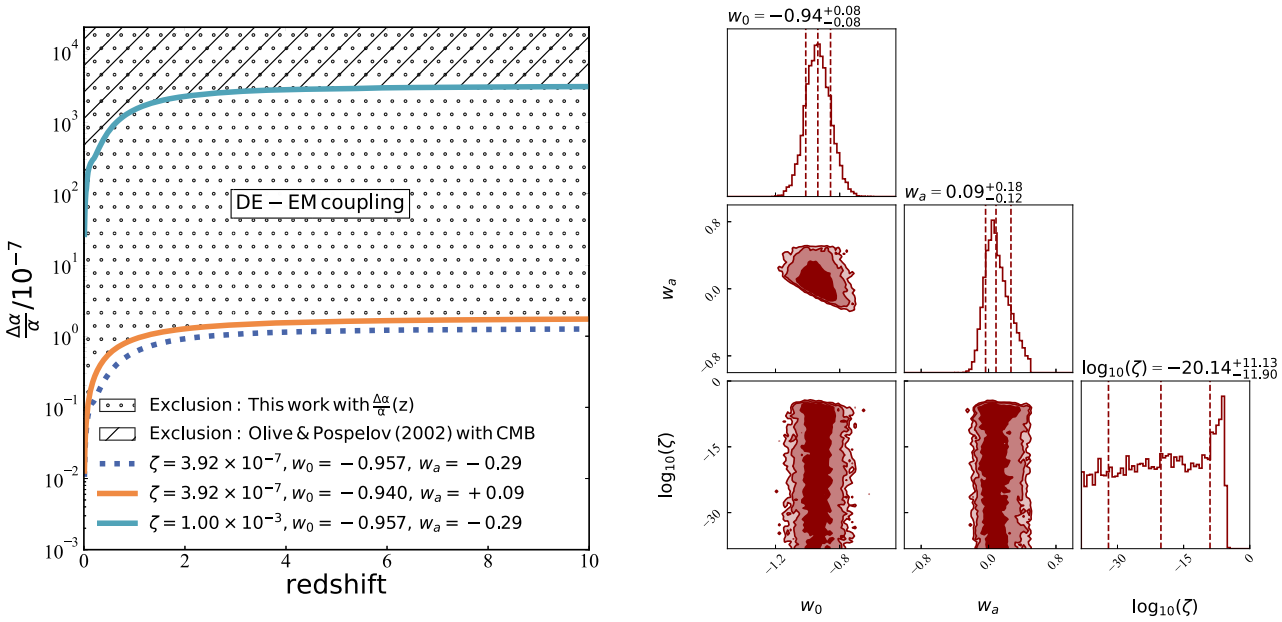

Figure 4. Left: The constraints on fine-structure constant evolution induced by dark energy coupling with electromagnetism. The lines in different styles and colors are constraints corresponding to different parameters. The area filled by slashes is the previous exclusion of $\zeta < 10^{-3}$ with CMB by Olive & Pospelov (2002). The area filled by dots is exclusion of this work. The parameters w_0 and w_a are free parameters of the dark energy equation of state in Equation (14). The parameter ζ is DE-EM coupling strength in Equation (13). Right: The posterior distribution of parameters of the DE-EM coupling model fitting to the combined $\frac{\Delta\alpha}{\alpha}(z)$ measurements.

they are still broader than those typically seen in galaxies. This broadening can lead to contamination of the Hβ lines, making it challenging to accurately determine the center of the lines (Bahcall et al. 2004; Jiang et al. 2024b). We cross-matched the current catalogs (Maiolino et al. 2024; Scholtz et al. 2023) of AGNs including the JADES data, and found there is one potential AGN in our sample. The source NIRSpec 10013905 was identified as a $z \sim 7.2$ AGN candidate by Scholtz et al. (2023) because of its [He II]λ4686 emission line. This optical He emission line could be from the ionized He by the ionizing radiation due to the central AGN. However, we find no strong evidence of the width of the [O III] doublet emission lines influenced by the AGN under the current uncertainty. Thus, that is not important to the current result.

Acknowledgments

This work is supported by the National Natural Science Foundation of China (NSFC, Grant Nos. 11921003, 12233011, and 12373002).

Appendix
Cornerplots of the MCMC Fitting

We produce the posterior distributions with Equations (3) and (9) in Figures A1, A2 and A3. The eight free parameters are a, b, λ_2, $\Delta\lambda$, n_1, n_2, s_1 and s_2. Clearly, the λ_2, $\Delta\lambda$, n_1, n_2, s_1 and s_2 are almost normally distributed. The plots only include the statistical uncertainties from the fitting. The analysis of systematic error is discussed in Section 3.

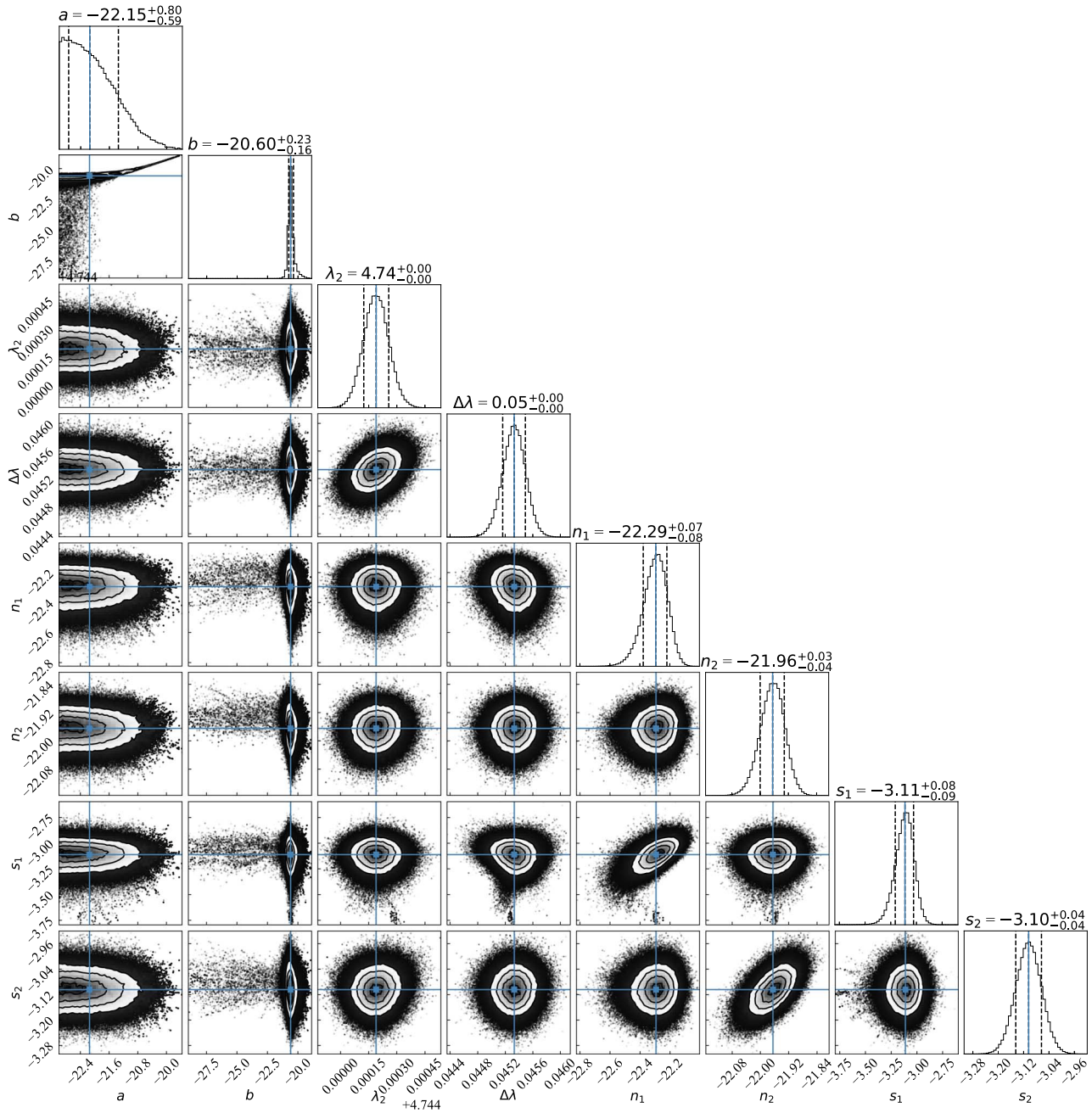

Figure A1. Posterior distribution of the parameters of NIRSpec 00008013. The diagonal figures are the posterior distributions of each parameter and the rest are joint distributions of one another. The blue solid lines are the 50% quantiles, and the dashed lines are for the 1σ range.

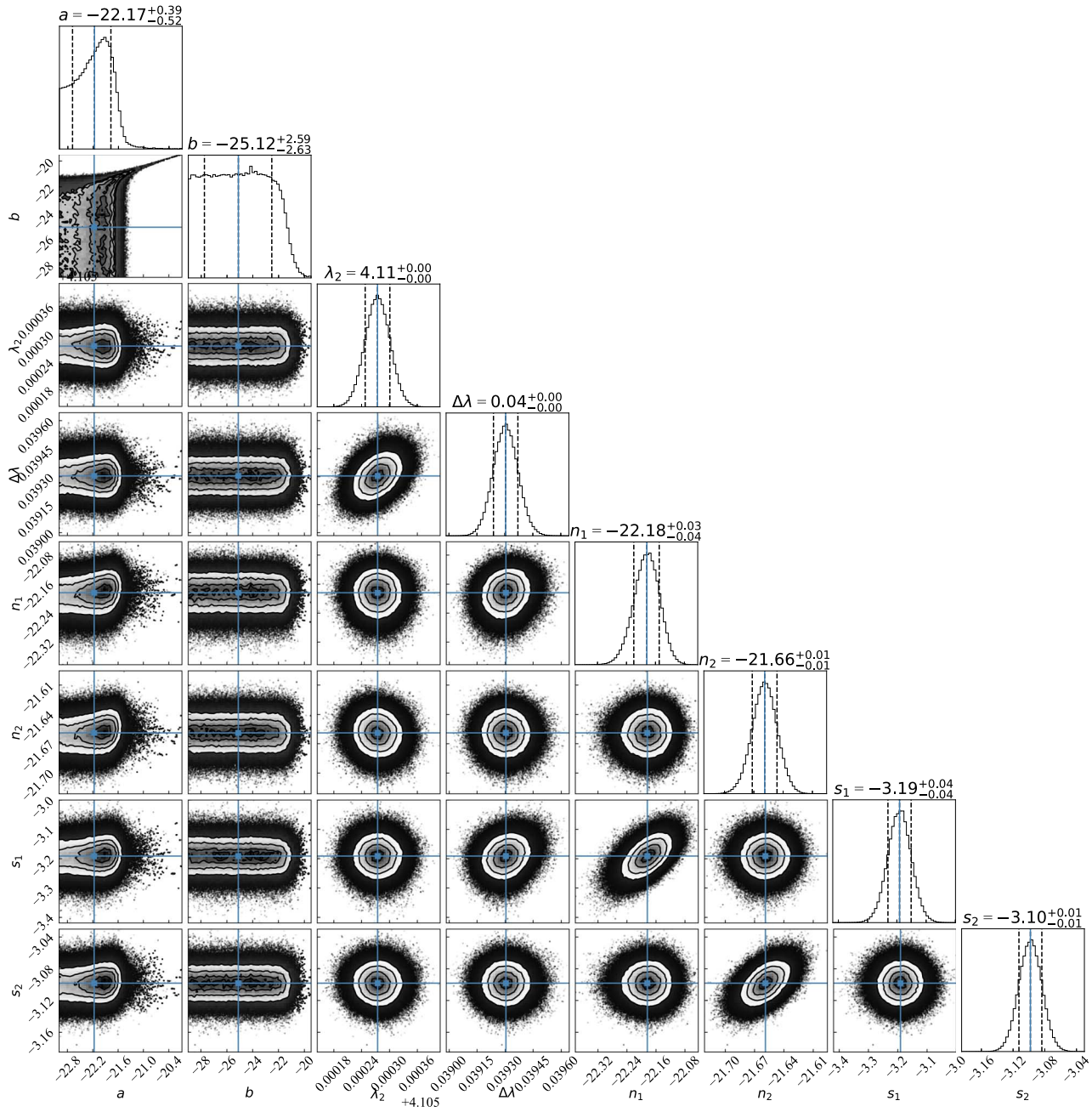

Figure A2. Posterior distribution of the eight parameters of NIRSpec 10013905.

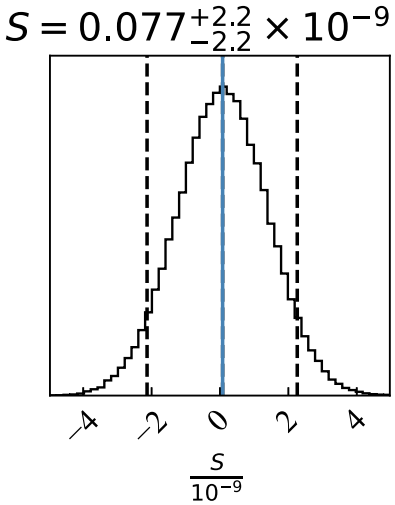

Figure A3. Posterior distribution of S. The blue solid line is the 50% quantile, and the dashed lines are for the 1σ range.

ORCID iDs

Ze-Fan Wang https://orcid.org/0009-0004-9366-1947
Lei Lei https://orcid.org/0000-0003-4631-1915

References

Alves, C. S., Leite, A. C. O., Martins, C. J. A. P., et al. 2018, PhRvD, 97, 023522
Avelino, P. P., Martins, C. J. A. P., Nunes, N. J., & Olive, K. A. 2006, PhRvD, 74, 083508
Bahcall, J. N., & Salpeter, E. 1965, ApJ, 142, 1677
Bahcall, J. N., Sargent, W. L., & Schmidt, M. 1967, ApJ, 149, L11
Bahcall, J. N., Steinhardt, C. L., & Schlegel, D. 2004, ApJ, 600, 520
Bunker, A. J., Cameron, A. J., Curtis-Lake, E., et al. 2024, A&A, 690, A288
Calabrese, E., Martinelli, M., Pandolfi, S., et al. 2014, PhRvD, 89, 083509
Chen, X., Ellingsen, S. P., & Mei, Y. 2019, RAA, 19, 018
Chevallier, M., & Polarski, D. 2001, IJMPD, 10, 213
Dirac, P. A. M. 1937, Natur, 139, 323
Dyson, F. J. 1967, PhRvL, 19, 1291
Eisenstein, D. J., Willott, C., Alberts, S., et al. 2023, arXiv:2306.02465
Foreman-Mackey, D., Hogg, D. W., Lang, D., & Goodman, J. 2013, PASP, 125, 306
Gamow, G. 1967, PhRvL, 19, 759
Jakobsen, P., Ferruit, P., Alves de Oliveira, C., et al. 2022, AA, 661, A80
Jiang, L., Fu, S., Wang, F., et al. 2024a, arXiv:2405.08977
Jiang, L., Pan, Z., Aguilar, J. N., et al. 2024b, ApJ, 968, 120
King, J. A., Webb, J. K., Murphy, M. T., et al. 2012, MNRAS, 422, 3370
Lee, D., Lee, W., Ng, K., et al. 2005, IJMPD, 14, 335
Linder, E. V. 2003, PhRvL, 90, 091301
Maiolino, R., Scholtz, J., Curtis-Lake, E., et al. 2024, A&A, 691, A145
Martins, C., & Pinho, A. 2017, PhRvD, 95, 023008
Miralda-Escudé, J. 1998, ApJ, 501, 15
Moorwood, A., Salinari, P., Furniss, I., Jennings, R., & King, K. 1980, A&A, 90, 304
Morel, L., Yao, Z., Cladé, P., & Guellati-Khélifa, S. 2020, Natur, 588, 61
Moss, A., Narimani, A., & Scott, D. 2010, IJMPD, 19, 2289
Mukhanov, V. F. 2005, Physical Foundations of Cosmology (Cambridge: Cambridge Univ. Press)
Nunes, N. J., & Lidsey, J. E. 2004, PhRvD, 69, 123511
Olive, K. A., & Pospelov, M. 2002, PhRvD, 65, 085044
Peck, E. R., & Reeder, K. 1972, JOSA, 62, 958
Petrov, Y. V., Nazarov, A. I., Onegin, M. S., Petrov, V. Y., & Sakhnovsky, E. G. 2006, PhRvC, 74, 064610
Pettersson, S.-G. 1982, PhyS, 26, 296
Planck Collaboration, Aghanim, N., Akrami, Y., et al. 2020, A&A, 641, A6
Robertson, B. E., Ellis, R. S., Dunlop, J. S., McLure, R. J., & Stark, D. P. 2010, Natur, 468, 49
Rosenband, T., Hume, D. B., Schmidt, P. O., et al. 2008, Sci, 319, 1808
Savedoff, M. P. 1956, Natur, 178, 688
Scholtz, J., Maiolino, R., D'Eugenio, F., et al. 2023, arXiv:2311.18731
Stanyukovich, K. 1963, SPhD, 7, 1150
Teller, E. 1948, PhRv, 73, 801
Thompson, R. I. 2013, MNRAS, 431, 2576
Topping, M. W., Stark, D. P., Endsley, R., et al. 2024, MNRAS, 529, 4087
Vielzeuf, P. E., & Martins, C. J. A. P. 2014, MmSAI, 85, 155
Webb, J. K., Flambaum, V. V., Churchill, C. W., Drinkwater, M. J., & Barrow, J. D. 1999, PhRvL, 82, 884
Webb, J. K., Murphy, M. T., Flambaum, V. V., et al. 2001, PhRvL, 87, 091301
Wilczynska, M. R., Webb, J. K., King, J. A., et al. 2015, MNRAS, 454, 3082
Wilczynska, M. R., Webb, J. K., Bainbridge, M., et al. 2020, SciA, 6, eaay9672
Wise, J. H. 2019, ConPh, 60, 145